Supporting information for

Unprecedented Nonphotomediated Hole (h^+) Oxidation System Constructed from Defective Carbon Nanotubes and Superoxides

Junhui Wang[a], Jiaxing Yu[b], Qi Fu[a], Huangsheng Yang[a], Qing Tong[c], Zhengping Hao[d], and Gangfeng Ouyang*[a,e]

[a] MOE Key Laboratory of Bioinorganic and Synthetic Chemistry, School of Chemistry, Sun Yat-Sen University, Guangzhou, Guangdong, 510275, China

[b] School of Materials Science and Engineering, Sun Yat-Sen University, Guangzhou, Guangdong, 510275, China

[c] Jiangsu Key Laboratory of Vehicle Emissions Control, Center of Modern Analysis, Nanjing University, Nanjing 210093, China

[d] National Engineering Laboratory for VOCs Pollution Control Material & Technology, University of Chinese Academy of Sciences, Beijing, 101408, China

[e] Chemistry College, Center of Advanced Analysis and Gene Sequencing, Zhengzhou University, Zhengzhou 450001, China

* Corresponding author:

Tel: +86 020 84110845/0953; fax: +86 020 84110845/0953.

E-mail address: cesoygf@mail.sysu.edu.cn (G. Ouyang)

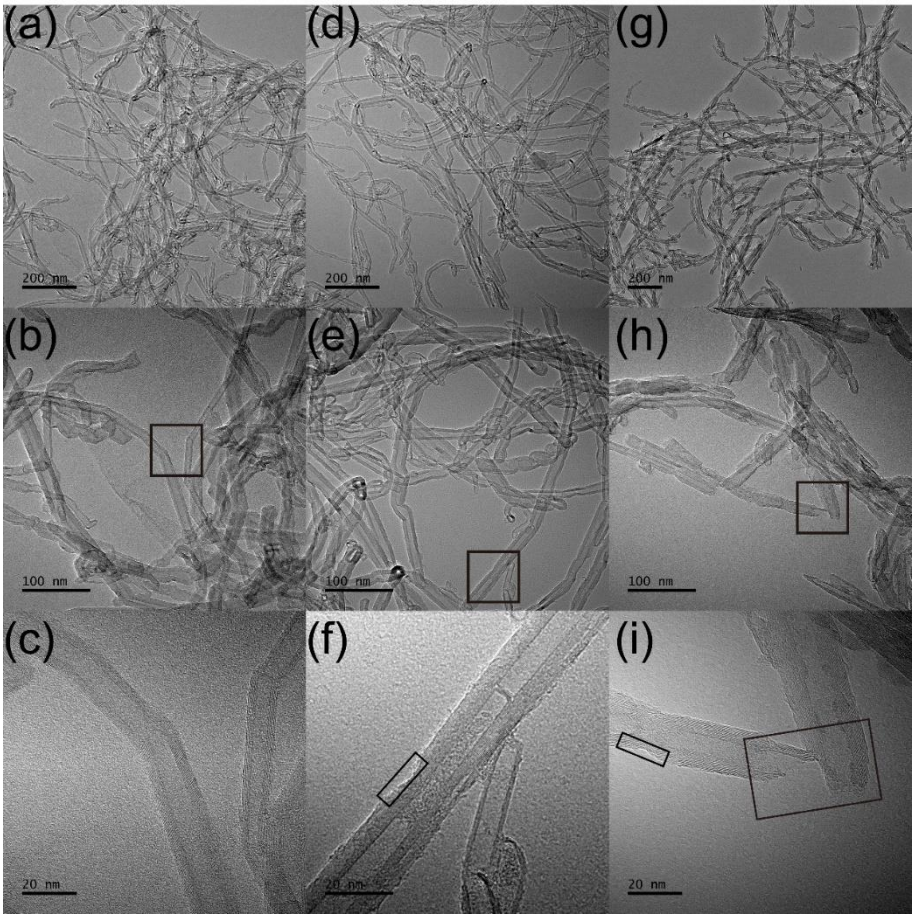

Figure S1. HRTEM images of G-CNT (a-c), ROCNT-3 (d-e) and ROCNT-6 (g-i). Images of (c), (f) and (i) are the magnifications of the squared regions in images of (b), (e) and (h), respectively. Squared regions in images (f) and (i) represent the defect sites etched by the acid oxidation.

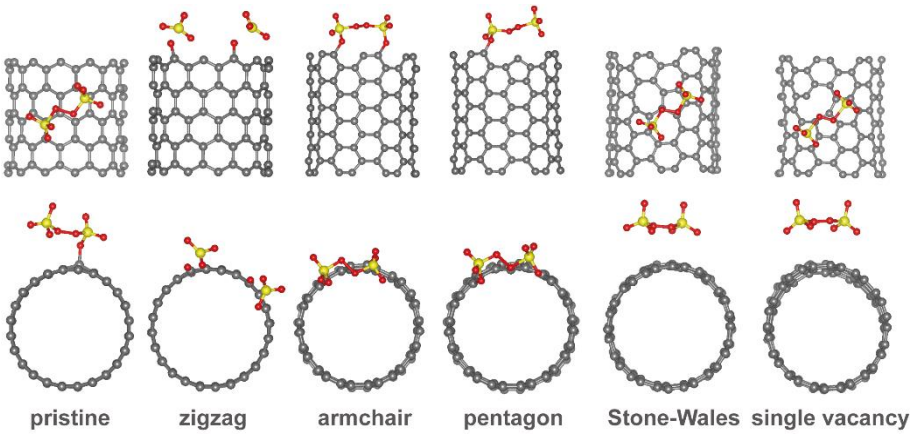

Figure S2. The favourite adsorption configuration of PS on pristine surface and different kinds of defects on CNT, respectively. Both the top view and side view are shown here.

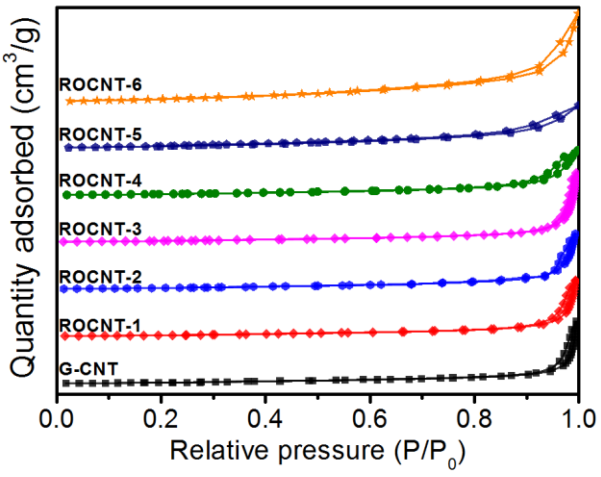

Figure S3. N_2 adsorption-desorption isotherms of CNT catalysts.

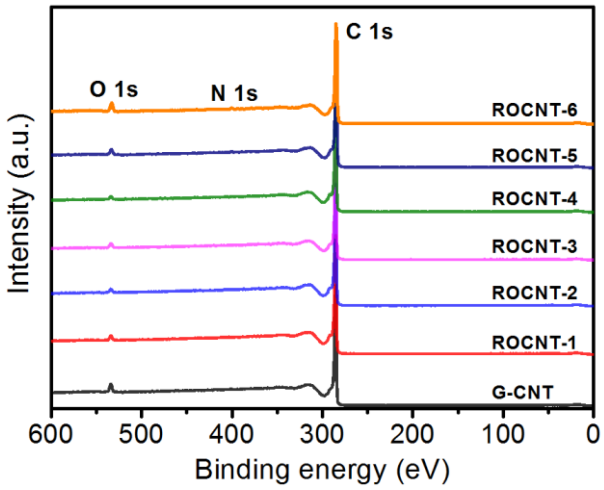

Figure S4. XPS spectra of CNT catalysts.

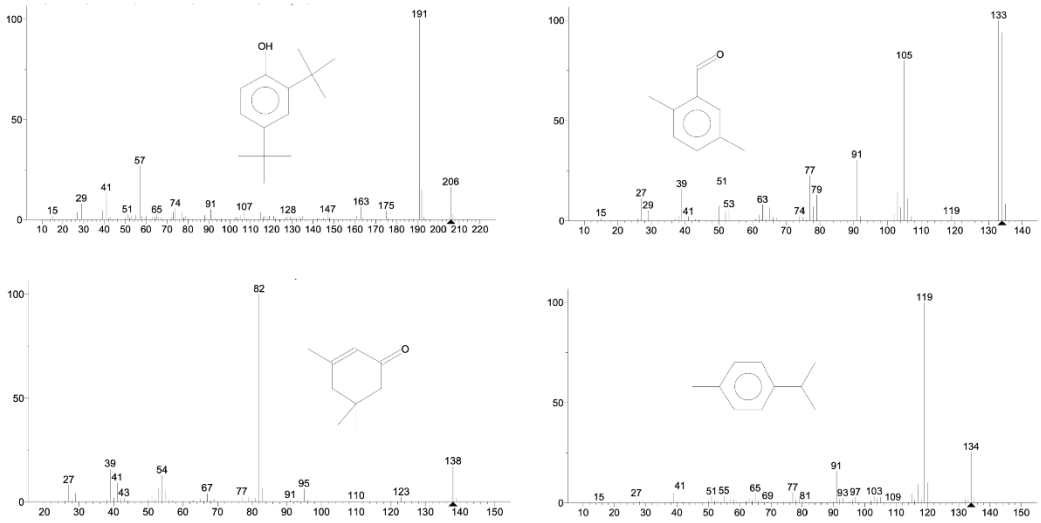

Figure S5. GC-MS spectra of the BPA degradation intermediates by the ROCNT-6/PS system.

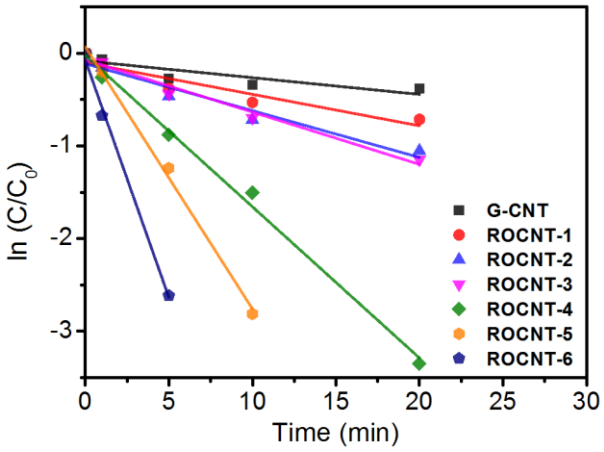

Figure S6. The kinetic analysis of BPA degradation on different CNT catalysts in the presence of PS according to pseudo-first-order model.

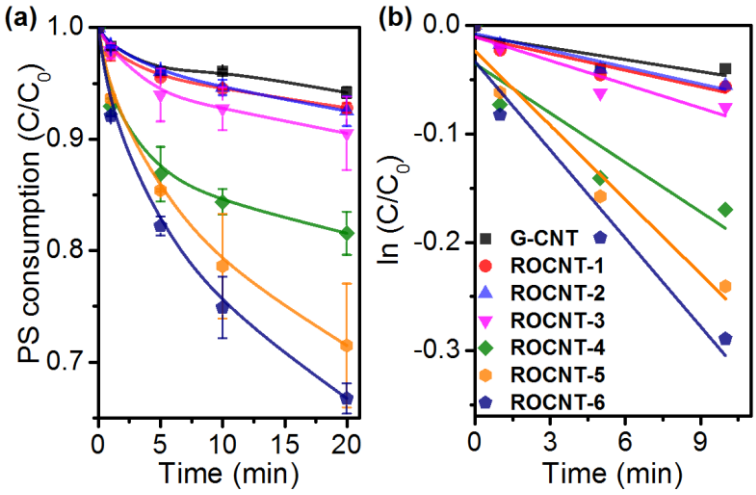

Figure S7. PS consumption on different CNTs (a) and the kinetic analysis of PS consumption according to pseudo-first-order model (b).

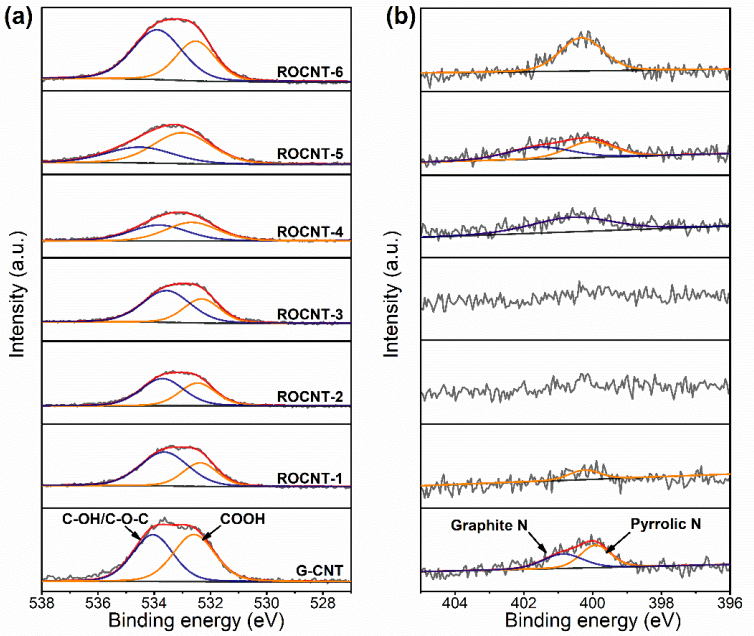

Figure S8. High-resolution XPS O 1s (a) and N 1s (b) spectra of the CNT catalysts.

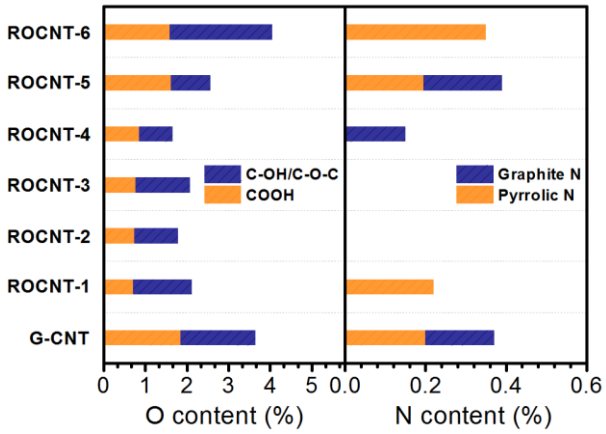

Figure S9. Contents of different O and N species on the CNT catalysts analyzed from XPS spectra.

XPS N 1s and O 1s spectra of the CNT catalysts were deconvoluted to quantify the types and contents of N and O species (Figure S8-9). It could be observed that the catalytic activities of ROCNTs had no positive correlation with neither N or O species.

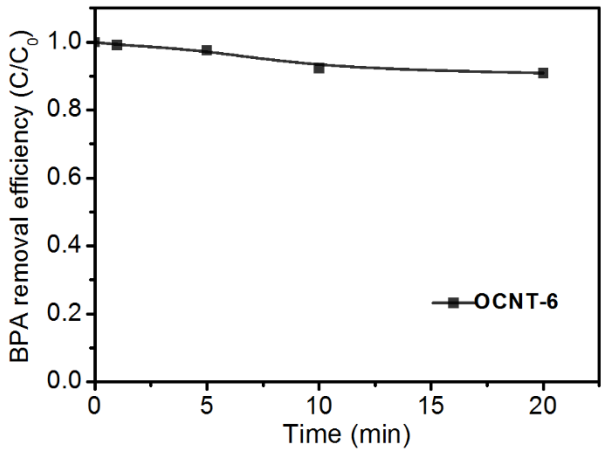

Figure S10. Catalytic degradation of BPA by OCNT-6. ([BPA]= 0.09 mM; [PS]=1.5 mM, [OCNT-6]=0.1 g/L)

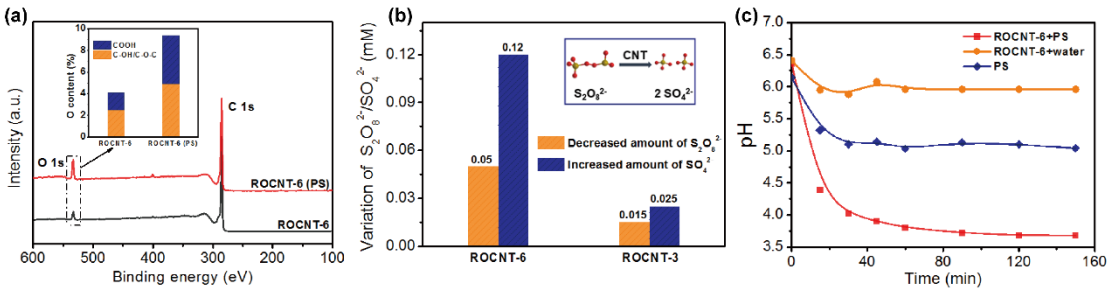

Figure S11. (a) XPS spectra and contents of O species of ROCNT-6 and ROCNT-6 treated with 1.5 mM PS solution for 1 h; (b) Variation of $S_2O_8^{2-}$ and SO_4^{2-} ions during the reaction of ROCNT-6/ROCNT-3 with PS solution for 1 h; (c) pH variation during the reaction process under different conditions. ([catalyst]=0.1 g/L; [PS]=0.15 mM)

As shown in Figure S11, ROCNT-6 was oxidized after treated with PS solution for 1 h. At the meantime, one PS molecular decomposed into two SO_4^{2-} ions, and water was the origin of the O species, due to the decrease of pH of the reaction solution.

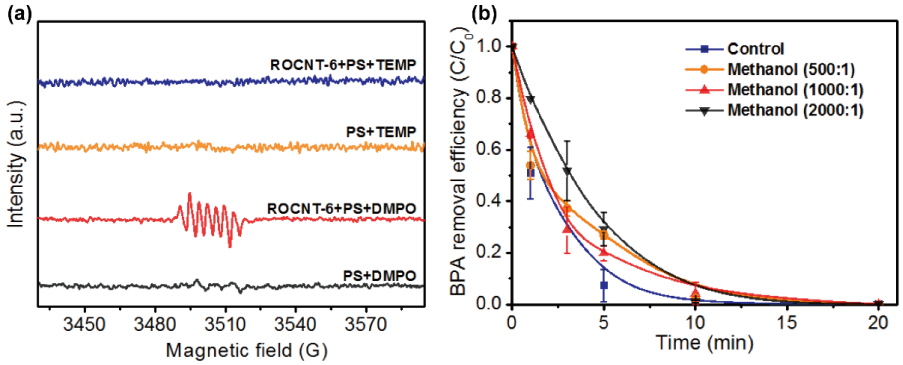

Figure S12. (a) EPR spectra obtained by spin trapping with DMPO and TEMP in the presence of PS and ROCNT-6 (reaction time=~5 min); (b) Degradation of BPA by the ROCNT-6/PS system with and without methanol. ([DMPO/TEMP]=10 mM; [ROCNT-6]=0.1 g/L; [PS]=1.5 mM)

EPR spin-trapping technique using 5,5-dimethyl-1-pyrroline N-oxide (DMPO) and 2,2,6,6-tetramethylpiperidine (TEMP) was applied to identify the active species produced in the ROCNT-6/PS system (Figure S12a). When DMPO was added as the spin-adduct, signals assigned to 5, 5-dimethyl-1-pyrrolidone-2-oxyl (DMPOX) were observed, which are distinguished from those of DMPO-$SO_4^{\cdot -}$ or DMPO-·OH, and always resulted from the oxidation of DMPO.[1-2] This DMPOX signal further indicated that there existed other kind of oxidative species in the reactions. Radical quenching experiments also confirmed that radical species merely contributed to the BPA degradation, because ROCNT-6 still maintained excellent BPA removal efficiency at a high concentration of methanol (2000:1) (Figure S12b). Moreover, no signals were obtained in the ROCNT-6/PS system using TEMP as the spin-adduct. These results indicate the presence of active species other than radicals ($SO_4^{\cdot -}$, ·OH) and singlet oxygen ($^1O_2$) during the reaction.

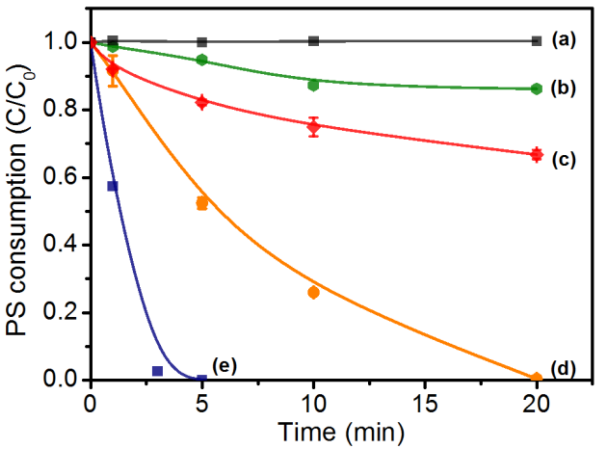

Figure S13. PS consumption under different conditions: (a) BPA+PS; (b) EDTA-2Na +PS; (c) ROCNT-6+PS; (d) ROCNT-6+BPA+PS; (e) ROCNT-6+EDTA-2Na+PS. ([ROCNT-6]=0.1 g/L; [PS]=0.15 mM; [BPA/EDTA-2Na]=0.09 mM)

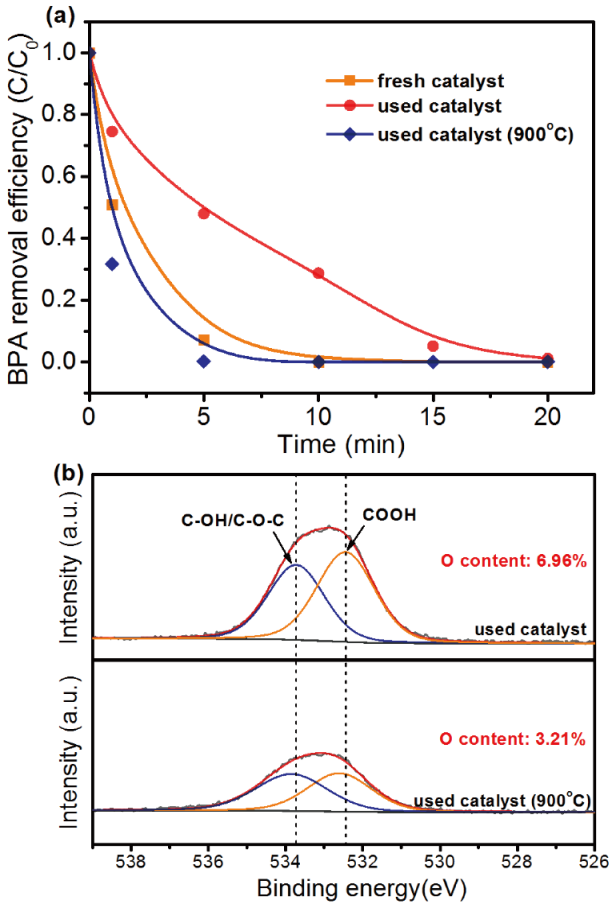

Figure S14. (a) The reusability investigation of ROCNT-6; (b) XPS 1Os spectra of used catalyst and regenerated catalyst after 900 ^{o}C treatment. ([BPA]= 0.09 mM; [ROCNT-6]=0.1 g/L, [PS]=1.5 mM)

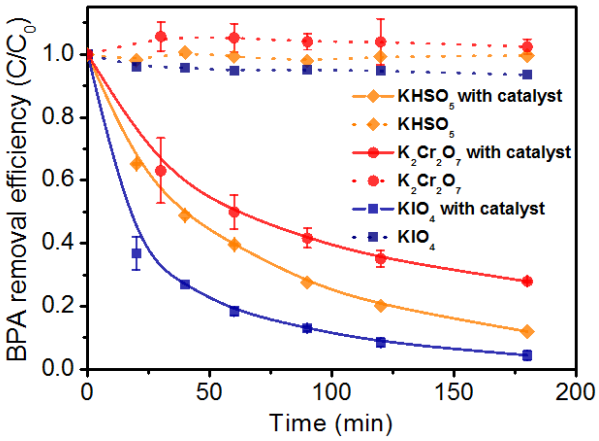

Figure S15. Catalytic degradation of BPA on ROCNT-6 with other different superoxides adsorbed. ([BPA]= 0.09 mM; [ROCNT-6]=0.1 g/L, [superoxide]=1.5 mM)

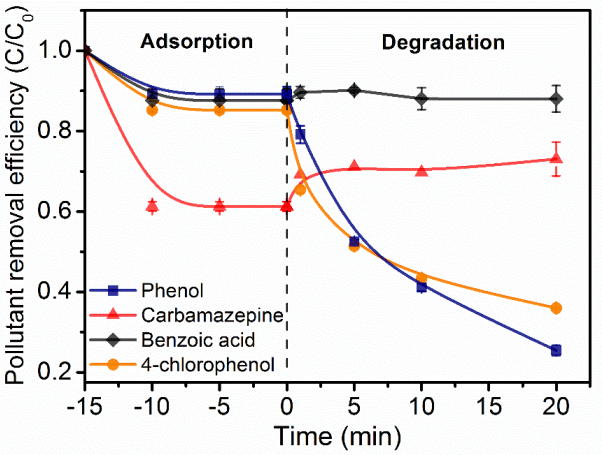

Figure S16. Catalytic performance of ROCNT-6/PS system for treating different pollutants (phenol, 4-chlorophenol, carbamazepine and benzoic acid) ([PS]=1.5 mM, [ROCNT-6]=0.1 g/L, [pollutant]=0.09 mM)

Table S1. Physicochemical parameters of the CNTs.

Catalyst	S_{BET} [a] (m^2/g)	O content [b] (wt%)	N content [b] (wt%)	BPA equilibrium adsorption amount, Q_e (mg/g)	Reaction rate constants, k_{BPA} (min^{-1})	Reaction rate constants, k_{PS} (min^{-1})
G-CNT	81	3.64	0.37	68	0.034	0.0037
ROCNT-1	89	2.11	0.22	58	0.034	0.0051
ROCNT-2	90	1.78	0	62	0.051	0.0052
ROCNT-3	95	2.07	0	68	0.056	0.0073
ROCNT-4	95	1.65	0.15	84	0.163	0.0152
ROCNT-5	101	2.57	0.39	115	0.283	0.0220
ROCNT-6	127	4.05	0.35	108	0.513	0.0270

[a] Brunauer-Emmett-Teller (BET); [b] Determined by XPS characterization.

Table S2. Comparison of recently reported photo/Fenton-like catalysts in BPA removal.

Name	Catalyst loading (g/L)	Reaction type	PMS [a]/H_2O_2 [b] (mM)	BPA concentration (mg/L)	Volume of treated solution (mL)	Removal efficiency	*k*-value (μmol/g/s)	Ref.
Co-BiOCl nanosheets	0.67	Photocatalysis	-	10	30	95% (120 min)	0.01	3
Ag_3PO_4@ $NiFe_2O_4$	0.25	Photocatalysis	-	10	80	100% (30 min)	0.10	4
Ag/SCN	0.6	Photocatalysis	-	10	50	100% (120 min)	0.01	5
OA-g-C_3N_4	0.4	Photocatalysis	-	15	50	100% (180 min)	0.02	6
$Bi_4O_5I_2$-Bi_5O_7I	1.0	Photocatalysis	-	10	50	94% (240 min)	0.003	7
$Fe_{0.8}Co_{2.2}O_4$	0.1	Fenton-like	0.2 [a]	20	50	95% (60 min)	0.23	8
$Fe_{0.15}Mn_{0.85}O_2$	0.04	Fenton-like	0.5 [a]	1.1	20	100% (15 min)	0.14	9
Fe(III)-g-C_3N_4	0.1	Fenton-like	1.0 [a]	23	100	95% (15 min)	1.06	10
$Mn_{1.8}Fe_{1.2}O_4$	0.1	Fenton-like	0.2 [a]	10	40	95% (30 min)	0.23	11
ce-MoS_2	0.015	Fenton-like	0.16 [a]	2	100	91% (10 min)	0.89	12
$Fe_1Mn_5Co_4$-N@C	0.1	Fenton-like	0.65 [a]	20	50	100% (12 min)	1.22	13
FeCo-NC-1	0.1	Fenton-like	0.2 [a]	20	100	100% (4 min)	3.65	14
CN-Cu(II)-$CuAlO_2$	1.0	Fenton-like	10 [b]	25	100	98% (120 min)	0.01	15
S modified Fe_2O_3	0.2	Fenton-like	0.04 [b]	44	100	100% (20 min)	0.80	16
ZIF-NC/ g-C_3N_4	0.1	Photo-Fenton -like	1.0 [a]	20	50	97% (60 min)	0.24	17
10%Ag/mpg-C_3N_4	0.1	Photo-Fenton -like	1.0 [a]	20	120	100% (60 min)	0.24	18
Ag/AgCl/Fh	1.0	Photo-Fenton -like	10 [b]	30	50	95% (30 min)	0.07	19
ROCNT-6	0.1	-	1.5 (PS)	20	20	93% (5 min)	2.72	This work

Table S3. Water quality parameters of Pearl River [a]

pH	TOC	Total nitrogen (mg/L)	NH_3-N (mg/L)	NO_3^- (mg/L)	NO_2^- (mg/L)	SO_4^{2-} (mg/L)	Cl^- (mg/L)
7.68	7.09	3.13	0.20	2.87	0.06	2.34	3.24

[a] Water samples were filtered by the 0.45 μm PTFE membranes to remove the particulate matters.

References

1. Lee, H.; Lee, H.-J.; Jeong, J.; Lee, J.; Park, N.-B.; Lee, C., Activation of persulfates by carbon nanotubes: Oxidation of organic compounds by nonradical mechanism. *Chem. Eng. J.* **2015,** *266*, 28-33.

2. Timmins, G. S.; Liu, K. J.; Bechara, E. J. H.; Kotake, Y.; Swartz, H. M., Trapping of free radicals with direct in vivo EPR detection: A comparison of 5,5-dimethyl-1-pyrroline-N-oxide and 5-diethoxyphosphoryl-5-methyl-1-pyrroline-N-oxide as spin traps for HO. and SO_4. *Free Radical Bio. Med.* **1999,** *27* (3-4), 329-333.

3. Wang, C. Y.; Zhang, Y. J.; Wang, W. K.; Pei, D. N.; Huang, G. X.; Chen, J. J.; Zhang, X.; Yu, H. Q., Enhanced photocatalytic degradation of bisphenol A by Co-doped BiOCl nanosheets under visible light irradiation. *Appl. Catal. B: Environ.* **2018,** *221*, 320-328.

4. Huang, S. Q.; Xu, Y. G.; Zhou, T.; Xie, M.; Ma, Y.; Liu, Q. Q.; Jing, L. Q.; Xu, H.; Li, H. M., Constructing magnetic catalysts with in-situ solid-liquid interfacial photo-Fenton-like reaction over Ag_3PO_4@$NiFe_2O_4$ composites. *Appl. Catal. B: Environ.* **2018,** *225*, 40-50.

5. Oh, W. D.; Lok, L. W.; Veksha, A.; Giannis, A.; Lim, T. T., Enhanced photocatalytic degradation of bisphenol A with Ag-decorated S-doped g-C_3N_4 under solar irradiation: Performance and mechanistic studies. *Chem. Eng. J.* **2018,** *333*, 739-749.

6. Qiu, P. X.; Xu, C. M.; Chen, H.; Jiang, F.; Wang, X.; Lu, R. F.; Zhang, X. R., One step synthesis of oxygen doped porous graphitic carbon nitride with remarkable improvement of photo-oxidation activity: Role of oxygen on visible light photocatalytic

activity. *Appl. Catal. B: Environ.* **2017,** *206*, 319-327.

7. Huang, H. W.; Xiao, K.; Zhang, T. R.; Dong, F.; Zhang, Y. H., Rational design on 3D hierarchical bismuth oxyiodides via in situ self-template phase transformation and phase-junction construction for optimizing photocatalysis against diverse contaminants. *Appl. Catal. B: Environ.* **2017,** *203*, 879-888.

8. Li, X.; Wang, Z.; Zhang, B.; Rykov, A. I.; Ahmed, M. A.; Wang, J., $Fe_xCo_{3-x}O_4$ nanocages derived from nanoscale metal–organic frameworks for removal of bisphenol A by activation of peroxymonosulfate. *Appl. Catal. B: Environ.* **2016,** *181*, 788-799.

9. Huang, K. Z.; Zhang, H., Direct electron-transfer-based peroxymonosulfate activation by iron-doped manganese oxide (δ-MnO_2) and the development of galvanic oxidation processes (GOPs). *Environ. Sci. Technol.* **2019,** *53* (21), 12610-12620.

10. Li, H. C.; Shan, C.; Pan, B. C., Fe(III)-Doped g-C_3N_4 mediated peroxymonosulfate activation for selective degradation of phenolic compounds via high-valent iron-oxo species. *Environ. Sci. Technol.* **2018,** *52* (4), 2197-2205.

11. Huang, G.-X.; Wang, C.-Y.; Yang, C.-W.; Guo, P.-C.; Yu, H.-Q., Degradation of bisphenol A by peroxymonosulfate catalytically activated with $Mn_{1.8}Fe_{1.2}O_4$ nanospheres: Synergism between Mn and Fe. *Environ. Sci. Technol.* **2017,** *51* (21), 12611-12618.

12. Chen, Y.; Zhang, G.; Liu, H.; Qu, J., Confining free radicals in close vicinity to contaminants enables ultrafast Fenton-like processes in the interspacing of MoS_2 membranes. *Angew. Chem.* **2019,** *131* (24), 8218-8222.

13. Li, X.; Ao, Z.; Liu, J.; Sun, H.; Rykov, A. I.; Wang, J., Topotactic transformation of

metal–organic frameworks to graphene-encapsulated transition-metal nitrides as efficient Fenton-like catalysts. *ACS Nano* **2016,** *10* (12), 11532-11540.

14. Li, X. N.; Huang, X.; Xi, S. B.; Miao, S.; Ding, J.; Cai, W. Z.; Liu, S.; Yang, X. L.; Yang, H. B.; Gao, J. J.; Wang, J. H.; Huang, Y. Q.; Zhang, T.; Liu, B., Single cobalt atoms anchored on porous N-doped graphene with dual reaction sites for efficient Fenton-like catalysis. *J. Am. Chem. Soc.* **2018,** *140* (39), 12469-12475.

15. Lyu, L.; Yan, D.; Yu, G.; Cao, W.; Hu, C., Efficient destruction of pollutants in water by a dual-reaction-center Fenton-like process over carbon nitride compounds-complexed Cu(II)-$CuAlO_2$. *Environ. Sci. Technol.* **2018,** *52* (7), 4294-4304.

16. Du, J. K.; Bao, J. G.; Fu, X. Y.; Lu, C. H.; Kim, S. H., Mesoporous sulfur-modified iron oxide as an effective Fenton-like catalyst for degradation of bisphenol A. *Appl. Catal. B: Environ.* **2016,** *184*, 132-141.

17. Gong, Y.; Zhao, X.; Zhang, H.; Yang, B.; Xiao, K.; Guo, T.; Zhang, J.; Shao, H.; Wang, Y.; Yu, G., MOF-derived nitrogen doped carbon modified g-C_3N_4 heterostructure composite with enhanced photocatalytic activity for bisphenol A degradation with peroxymonosulfate under visible light irradiation. *Appl. Catal. B: Environ.* **2018,** *233*, 35-45.

18. Wang, Y. B.; Zhao, X.; Cao, D.; Wang, Y.; Zhu, Y. F., Peroxymonosulfate enhanced visible light photocatalytic degradation bisphenol A by single-atom dispersed Ag mesoporous g-C_3N_4 hybrid. *Appl. Catal. B: Environ.* **2017,** *211*, 79-88.

19. Zhu, Y. P.; Zhu, R. L.; Xi, Y. F.; Xu, T. Y.; Yan, L. X.; Zhu, J. X.; Zhu, G. Q.; He, H. P., Heterogeneous photo-Fenton degradation of bisphenol A over

Ag/AgCl/ferrihydrite catalysts under visible light. *Chem. Eng. J.* **2018,** *346*, 567-577.